In-plane Detection of Guided Surface Plasmons for High Speed Optoelectronic Integrated Circuits

Evgeniy Panchenko*[1,2], Jasper J. Cadusch[1], Ori Avayu[3], Tal Ellenbogen[3], Timothy D. James[1], Daniel Gómez[2,4], and Ann Roberts[1]

[1]*School of Physics, University of Melbourne, Victoria 3010, Australia*

[2]*Melbourne Centre for Nanofabrication, Australian National Fabrication Facility, Clayton, Victoria 3168, Australia*

[3]*Department of Physical Electronics, School of Electrical Engineering, Tel Aviv University, Tel Aviv 61000, Israel*

[4]*RMIT University, Victoria 3000, Australia*

Abstract

Constrains on the speed of modern digital integrated circuits are dominated by the metallic interconnects between logic gates. Surface plasmon polaritons have potential to overcome this limitation and greatly increase the operating speed of future digital devices. Nevertheless, an ongoing issue is the compatibility of modern planar microelectronic circuits with current methods for detecting surface plasmons. Here we propose and experimentally demonstrate a new approach to in-plane surface plasmon polariton detection. The design is based on metal-semiconductor-metal photodetectors which are acknowledged as having one of the best speed characteristics among photodetectors. In our design, the photodetector structure also plays a dual role as the outcoupling grating for surface plasmons, significantly reducing the footprint of the resulting device. Our technique has the potential to enable the

*evgeniy.panchenko@unimelb.edu.au

integration of surface plasmons as signal carriers in future high-speed optoelectronic integrated circuits.

The ever-increasing demand for high-speed data processing requires faster operation of computer processors (CPU) and peripherals. This becomes extremely important when performing sequential tasks that cannot be parallelised across multiple computational nodes (e.g cryptography and non-linear simulations). Despite the gradual improvement in semiconductor technology processes [1] (such as the decrease in transistor gate dimensions) which, in turn, should lead to a corresponding increase in the frequency of logic gate switching, the speed of modern CPUs has remained relatively constant. Since the switching speed of discrete transistors can be very high [2, 3] the constraint, therefore, lies outside the logic gates and is primarily determined by metallic interconnects in integrated circuits [4]. The underlying phenomenon is a signal propagation delay - a physical limit of the propagation velocity of the electrical signal in the chip. In microelectronics it is dominated by the RC time constant [5]. The bandwidth and the speed of the interconnect is reduced by the time required to charge a parasitic capacitance of the interconnect. This RC constant, therefore, defines the speed limit of the microelectronic circuit regardless of the speed of each individual logic gate. Numerous enhancements have been introduced to conventional CMOS technology such as substitution of Al interconnects with Cu [6, 7] and the utilisation of low-k dielectrics [8] for interlayer insulation in order to decrease the resistance and capacitance of the interconnects. Even though these changes have markedly improved the characteristics of interconnects, further developments of this technology are extremely challenging and cost-ineffective. Therefore, as the current technology is rapidly reaching its limits, a new approach is required to overcome the existing issues and build high-speed digital devices.

Recent research in silicon photonics has demonstrated the potential for using light as a signal carrier, not only for long-distance communications, but also for on-chip interconnects. Various optical elements such as waveguides [9, 10, 11, 12, 13], modulators [14, 15, 16, 17] and filters [17, 18] have been successfully integrated into microelectronic

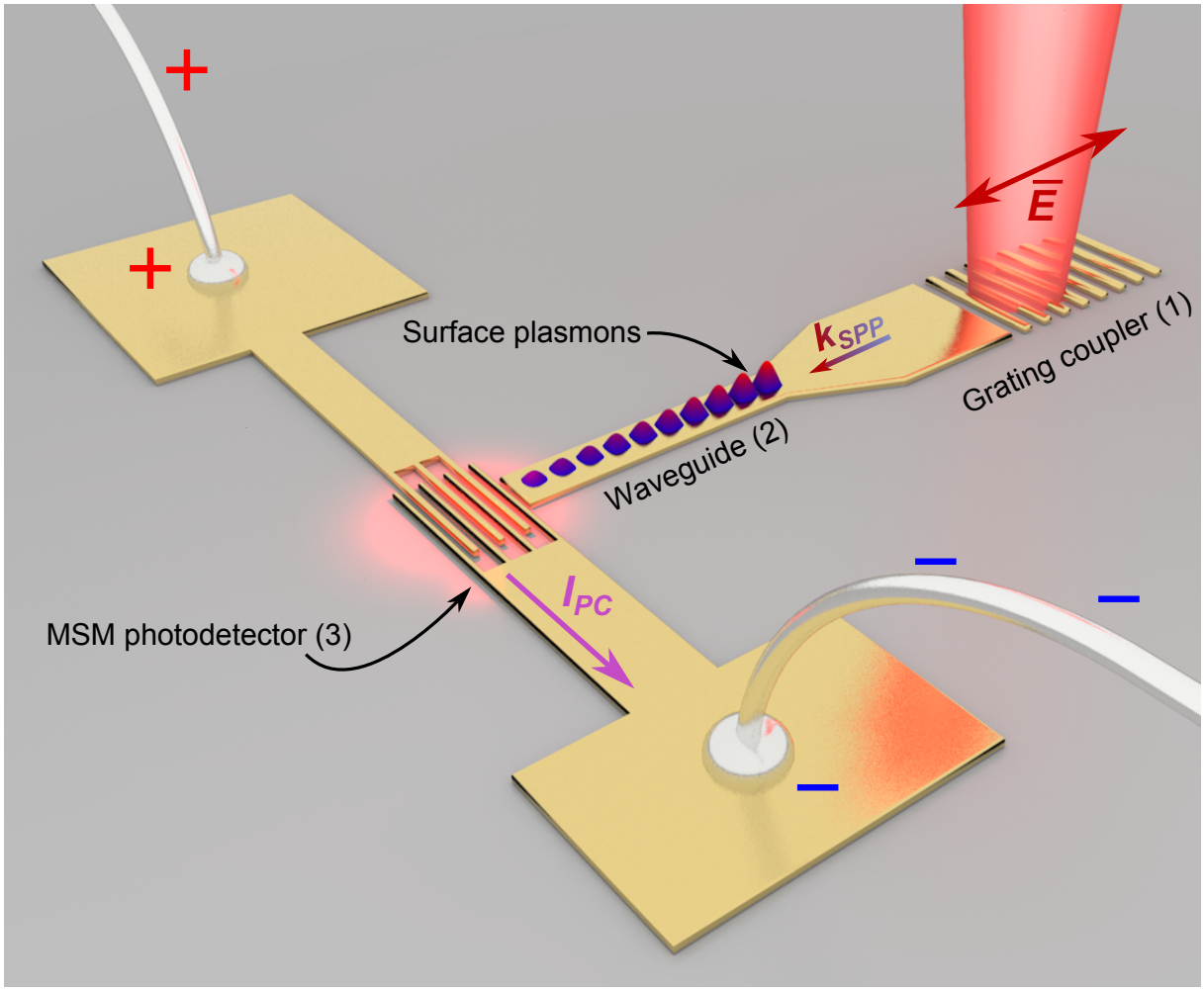

Figure 1: Schematic representation of a waveguide-coupled metal-semiconductor-metal (MSM) photodetector with excitation grating. Surface plasmons are excited using a grating coupler **(1)** and tapered into a stripe waveguide **(2)** which is coupled to a metal-semiconductor-metal photodetector **(3)**. When a surface plasmon reaches detector grating it outcouples into the substrate and generates electron-hole pairs. These carriers are swept by electric field under the photodetector resulting in photocurrent I_{PC} generation.

circuits. Another promising technology for signal processing, in terms of very-large-scale integration (VLSI), is the emerging field of plasmonics. It utilises surface plasmons which are oscillations of the electron gas at the interface between metal and dielectric. The ability of surface plasmons to circumvent the conventional optical diffraction limit [19, 20] as well as providing strong field confinement [21, 11, 22] opens up significant opportunities for using them to guide signals between logic gates in modern integrated circuits where small dimensions are highly desirable. Moreover, the high sensitivity of surface plasmons to the properties of surrounding media compared to purely photonic elements permits the

design of submicron active components by modulating the optical environment. Passive devices such as wave plates [23], filters [24] and logic gates [25] as well as active elements such as tunable antennas [26, 27] and detectors [11, 28, 29, 11, 13] utilising plasmonic phenomena, have been demonstrated.

In order to utilise surface plasmon polaritons (SPPs) as signal carriers it is essential to provide a reliable detection mechanism. Numerous SPP detection techniques using nanowires [20] or metal-insulator-metal waveguides [30, 11] have been recently reported. Although these approaches showed a good capacity for detecting surface plasmons, their practical application is limited by the complexity of design and fabrication. For smooth integration of plasmonic interconnects with detectors a planar geometry and reproducible characteristics are essential. Furthermore, for modern electronic applications, minimising the device footprint is critical.

Here we propose a nanoscale alternative, based on a metal-semiconductor-metal photodetector coupled to a plasmonic waveguide (see Fig.1). When a surface plasmon reaches the detector grating it outcouples into the substrate and generates electron-hole pairs which produce a photocurrent. A device such as this performs *in-plane* SPP detection and could form one of the building blocks of future high-speed optoelectronic integrated circuits.

Metal-semiconductor-metal (MSM) photodetectors are commonly used in ultrafast optoelectronic devices. It has been shown that Si-based MSM photodetectors can operate up to a frequency of 140 GHz [31], demonstrating that very high-speed operation can be achievable. It was also shown [32] that by utilising the properties of plasmonic structures it is possible to design photodetectors that are sensitive to the polarisation state of an incident optical beam. It should be noted that such a high speed comes at the cost of a low responsivity [33]. The responsivity of proposed MSM photodetector design is approximately 9.2 mA/W.

1 Device structure and functionality

A typical band diagram of an MSM photodetector under reverse bias is shown in Figure 2a. The detector consists of two interdigitated metal electrodes (see Fig.2b) deposited on a low-doped semiconductor. Each of these electrodes forms a Schottky barrier with the substrate. Since the substrate is common, the MSM photodetector represents two Schottky diodes connected back-to-back (see Fig.2c). Such photodetector is, therefore, bi-directional and will always operate under reverse bias independent of which electrode is at the higher potential. The photodetector presented here is capable of detecting photocurrent generated by both hot-electrons and electron-hole pairs.

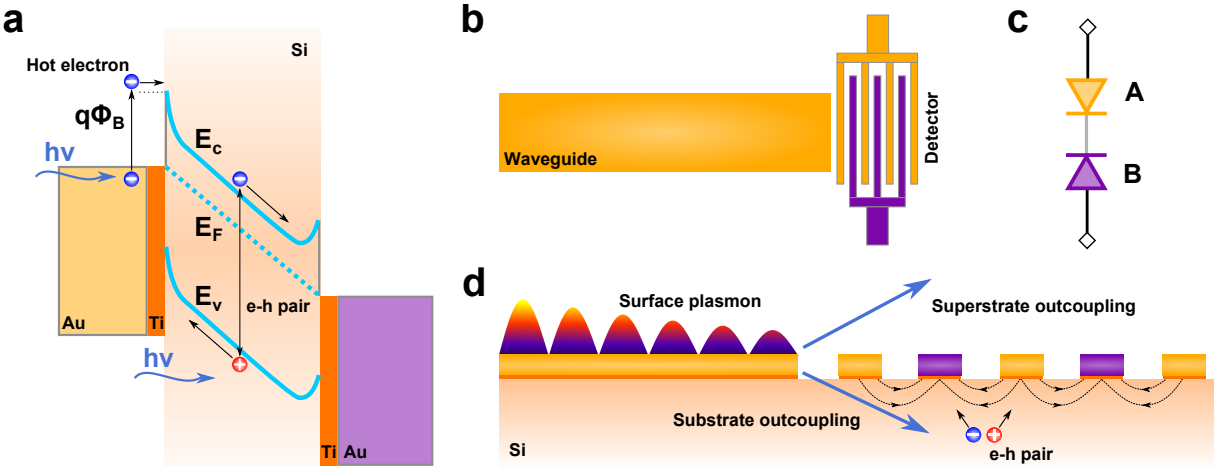

Figure 2: A band diagram of biased MSM photodetector **(a)** describing two possible mechanisms of photocurrent generation. $q\Phi_B$ is a height of the Schottky barrier, E_v, E_c and E_F are valence, conduction and Fermi energy levels respectively. Schematic representation of MSM photodetector coupled with waveguide **(b)** and equivalent electric circuit of the detector **(c)**. The surface plasmon outcoupling mechanism on MSM photodetector **(d)**.

The device is implemented on a silicon substrate with a bulk resistivity of 1-10 Ω·cm. A 85 nm thick layer of gold was used as a waveguide material deposited on a 2 nm thick titanium adhesion layer (see Fabrication section). Surface plasmons are excited in a 5 µm wide waveguide using grating coupling. A grating was designed for a normally incident plane wave at 635 nm with a period of 600 nm. It was numerically demonstrated that grating couplers can exhibit efficiency up to 50% [34]. The operating wavelength was

chosen to be in the visible part of the EM spectrum (albeit at the red end to minimise losses) as the electron-hole pair generation is a much a more efficient process than hot-electron injection and leads to more efficient photodetection. We were able to verify the excitation and guiding of surface plasmons by monitoring scattering by the MSM grating using a CCD camera. The depth of the grating is identical to the thickness of the metal film and is equal to 85 nm. This thickness was chosen to ensure the top and bottom modes were decoupled and to reduce leakage of surface plasmons into the substrate [9]. The excitation section is then tapered into a 2.5 µm wide asymmetric stripe waveguide which, in addition to a fundamental mode, can support several higher order modes at this wavelength. The width chosen is a compromise, balancing loss while minimising size. The waveguide is used to deliver surface plasmons to the active zone of the MSM photodiode. The expansion of the waveguide leads to a reduction in the attenuation constant and an increase in the SPP propagation length.

Several phenomena are simultaneously contributing to the photocurrent generated by this device. The fingers of the detector can couple surface plasmons back into radiation (see Fig.2d) allowing photons to penetrate into the substrate. If the photon energy is above the band gap of the semiconductor ($h\nu > E_{bg}$) it will be absorbed resulting in electron-hole pair generation. The energy of generated electrons in this case is by definition larger than the energy of the Schottky barrier which the electrons can overcome (since the metal-semiconductor barrier is smaller than the bandgap of the semiconductor [35]). Furthermore, surface plasmons can nonradiatively decay in the metal fingers [36] and be absorbed in them. This in turn, will lead to hot-electron generation and injection through the Schottky barrier into the substrate. Such a device, therefore, permits the detection of surface plasmons with energies, both above and below the band gap of a semiconductor.

Applying a bias to the electrodes of the detector leads to the formation of an electric field gradient (see Fig.2d) in the active zone under the fingers. Every charge carrier generated or injected into the semiconductor substrate will be swept by this electric field to the top electrode resulting in a photocurrent flowing through the device. Since

the device operating wavelength is in the visible part of the spectrum, so the photons have energies above the Si bandgap, both electron-hole pairs generation and hot-electron injection will contribute to the generated photocurrent. The influence of hot electron injection, however, is neglected due to the much lower efficiency compared with direct photon absorption in Si.

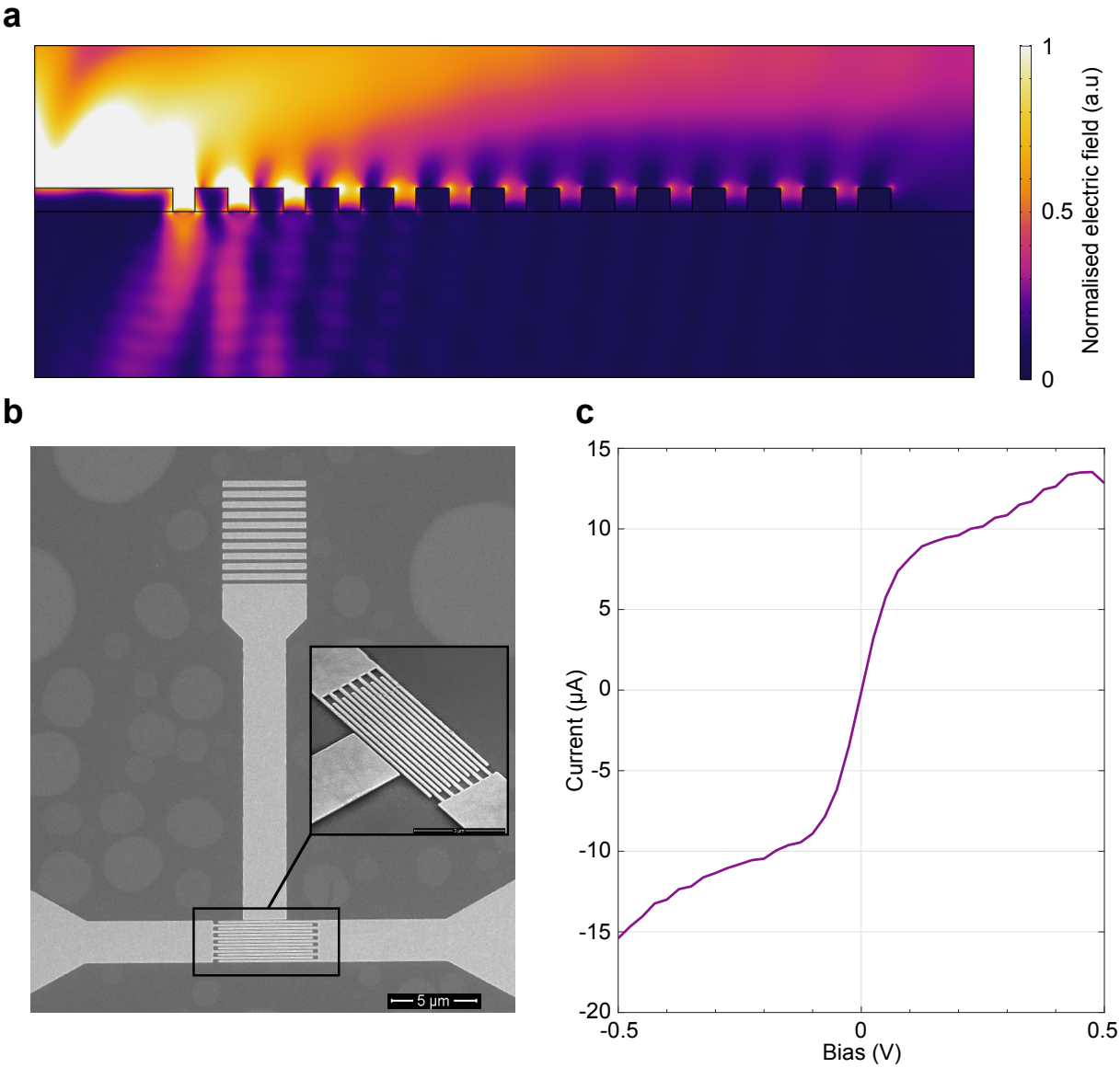

Figure 3: Normalised electric field distribution in the MSM photodetector active region **(a)**. A period of 200 nm and duty cycle of 0.6 were used in simulation. SEM image **(b)** and measured I-V curve **(c)** of the waveguide-coupled MSM photodetector. Inset shows a close-up of the MSM photodetector grating at 30° tilt.

To optimize the sensitivity of the device a Finite Element Method (FEM) simulation

(see Simulation section) was performed to determine the relationship between the irradiance delivered to the photodetector active region (see Fig.3a), the separation between the fingers and the grating duty cycle (for more information see Supplementary Materials). The outcoupling of surface plasmons into the substrate involves two effects: a momentum transfer provided by the MSM grating and the localised plasmon resonance of each finger which enhances the radiation. Increasing the period while keeping the duty cycle fixed, increases the separation of the fingers, weakening the near-field coupling of each finger with its neighbours which, in turn, decreases the power flow into the substrate. The same tendency can be observed in the case of large duty cycles. This can be explained by the narrowing of the slits through which the surface plasmons outcouple into the substrate. Considering these results together with fabrication limitations, a grating with a duty cycle of 0.6 and a period of 200 nm (see Fig.3b) was chosen. The photodetector consists of 13 fingers giving an active area of 13.75 µm^2.

The capacitance per unit area of an MSM photodetector can be calculated using the following expression [37]:

$$C_{MSM}(W,G) = \frac{K(k)}{K(\sqrt{1-k^2})} \frac{\epsilon_0(\epsilon_s + \epsilon_d)}{W+G}, \tag{1}$$

where ϵ_s and ϵ_d are the dielectric permittivities of the semiconductor and cladding respectively, W and G are the widths of the fingers and the gaps between them, and K is the complete elliptic integral of the first kind with:

$$k = \tan^2\left(\frac{\pi W}{4(G+W)}\right). \tag{2}$$

With the parameters above, equation (1) gives a capacitance per unit area of the MSM photodetector of 3.071x10^{-4} Fm^{-2}. Assuming that the photodetector is connected to a 50 Ω impedance load gives the maximum theoretical bandwidth of approximately 750 GHz.

2 Device characterisation

The dark I-V characteristic of the photodetecor is shown in Figure 3c. As previously mentioned, the detector consists of two identical Schottky diodes connected back-to-back and, therefore, shows similar behavior under both positive and negative bias. The curve saturates around 0.1 V which means that the Schottky barrier height is lower than usually reported for Ti-Si contacts [38, 39]. This can be explained by imperfections introduced during the fabrication process since there are a number of factors that can affect the height of the barrier such as contamination of the Si surface, quality of the metal film and the inevitable formation of an ultra-thin layer of native oxide prior to the metal evaporation. For simplicity the contact pads (250 µm^2 each) were deposited onto the silicon in the same fabrication step with the detector fingers. As a consequence, the detector exhibits a relatively large dark current due to the large metal-semiconductor contact area. The dark current could be reduced by lifting the pads above the substrate by introducing a thick silica layer or p-wells underneath and including guard rings around the metal edges.

The fingers of the photodetector act as a decoupling grating enabling the observation of surface plasmons by scattering. An MSM photodetector coupled to a 16.75 µm long waveguide was chosen for observation (see Fig.4a). The laser beam was focused onto the in-coupling grating and a half-wave plate used to control beam polarisation. The reflected image was captured using a CMOS camera. The normalised scattering intensity as a function of polarisation is shown on Figure 4b. The scattering intensity exhibits the expected $\cos^2(\theta)$ behaviour, where θ is the angle of polarisation measured relative to the perpendicular to the grating lines. As can be seen from Figure 4c,d the scattering from the MSM photodetector fingers is maximal when the electric field of the incident beam is perpendicular to the lines of the in-coupling grating (TM polarisation), which confirms the excitation and guiding of the surface plasmons in the waveguide. Near-field scanning optical microscopy (NSOM) measurements were performed to further confirm surface plasmons guiding and to optimise waveguide design (for more information see Supplementary Materials).

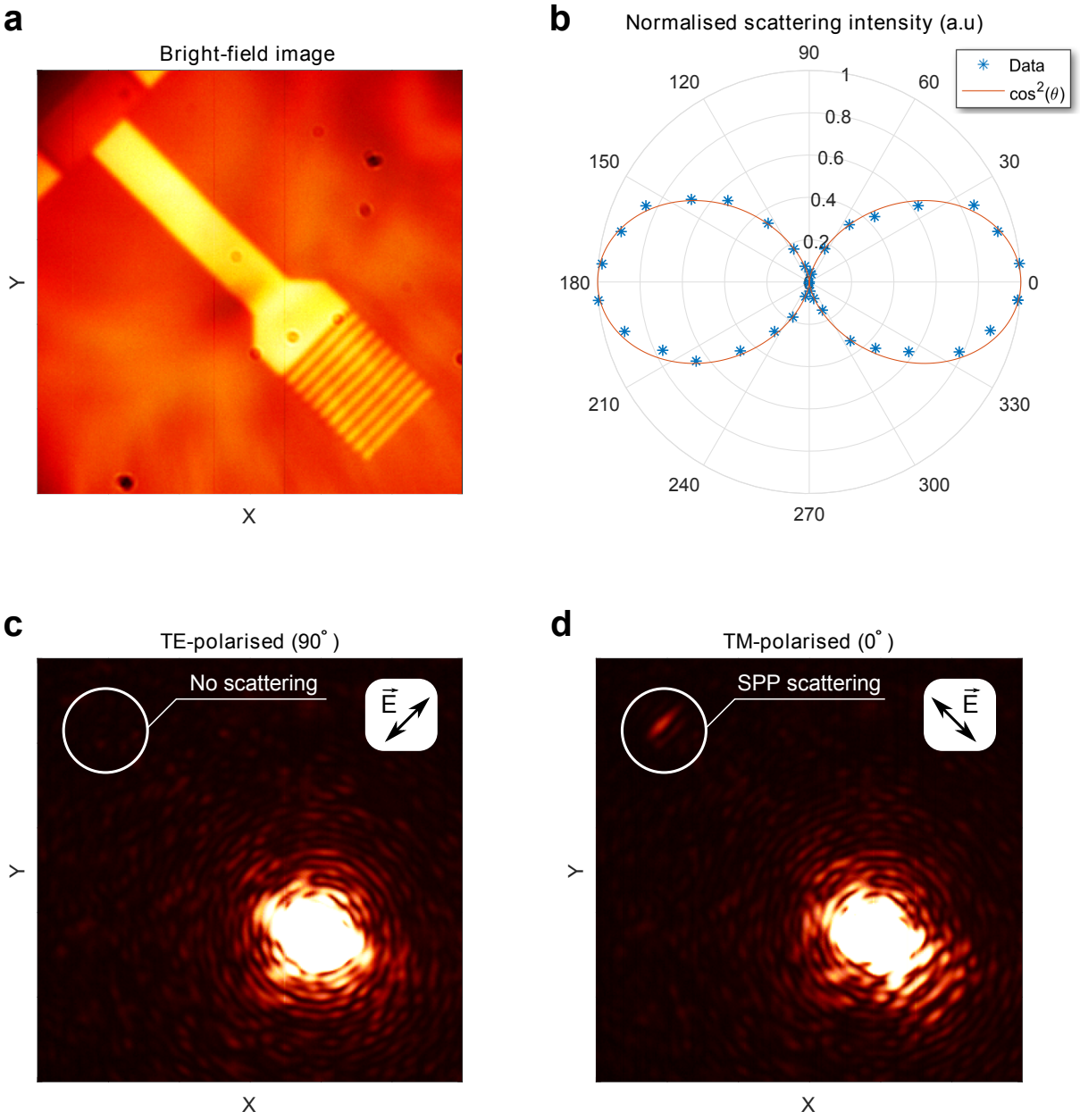

Figure 4: Bright-field image of a waveguide-coupled MSM photodetector **(a)**. Dependence of the normalized scattering intensity from MSM fingers from polarisation of the excitation beam **(b)**. Scattering from the fingers (circled) of 2.5 µm wide waveguide-coupled MSM photodetector for TE ($\theta = 90°$) **(c)** and TM ($\theta = 0°$) **(d)** polarisation of the excitation beam respectively.

Scanning photocurrent microscopy (SPCM) [40] was used to confirm the functionality of the device. A 11.75 µm long waveguide-coupled MSM photodetector (see Fig.5a) was biased at 0.15 V and the generated photocurrent was collected and correlated with the position of the beam. Images were obtained for both TE ($\theta = 90°$) and TM ($\theta = 0°$)

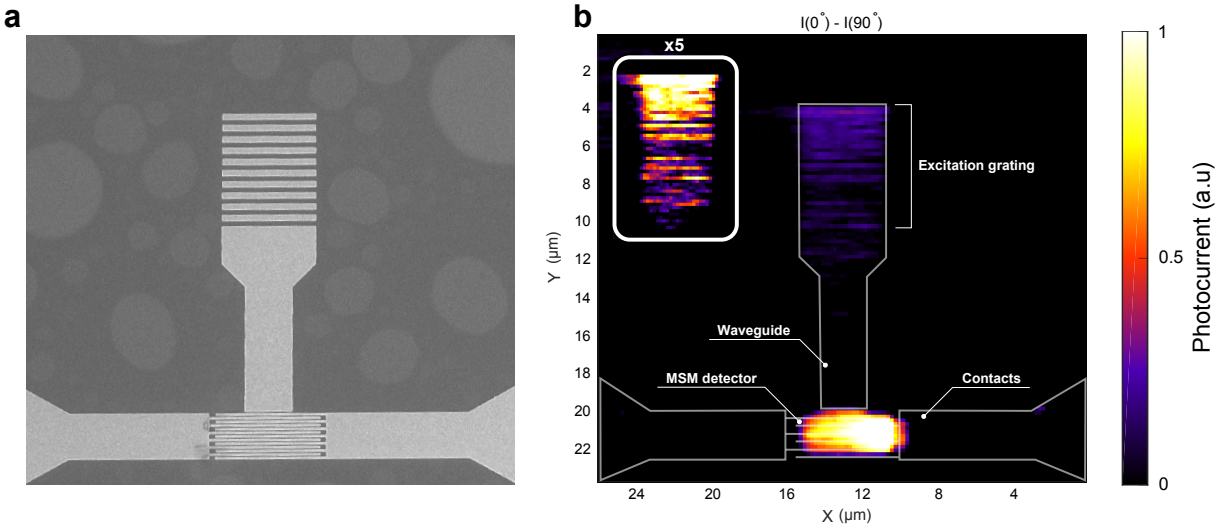

Figure 5: SEM image of an MSM photodetector coupled to 11.75 µm long waveguide **(a)** and difference of scanning photocurrent maps obtained under TM (0°) and TE (90°) polarised 635 nm laser beam **(b)**. Colour scheme range in the inset is decreased by a factor of 5 for clarity.

polarised incident light and the photocurrent maps were then normalised and subtracted one from another I(TM)-I(TE) (see Fig.5b). As can be seen, the photocurrent is maximal when either the active zone of photodetector (due to the direct photon detection) or the excitation grating are illuminated. In the case of the in-coupling grating illumination, the generated photocurrent is higher for TM-polarised light due to surface plasmon excitation and subsequent detection by the MSM photodetector (see Fig.5b). This confirms that the increase in the photocurrent near to the excitation grating is caused by the outcoupling of the surface plasmons into the photodetector active region.

Since the insulator-metal-insulator (IMI) waveguide structure [9] utilised in this device exhibits a strong attenuation constant due to its vertical asymmetry (the superstrate has a much smaller dielectric constant than the substrate), the intensity of the surface plasmons decays strongly as they propagate along the waveguide. To investigate the decay of surface plasmons, four identical waveguide-coupled photodetectors with different lengths were fabricated and characterized using a similar setup to which was used to obtain the scattering images. The laser beam was focused onto the coupling grating to excite surface plasmons on the waveguide. The photocurrent from the detector was recorded during

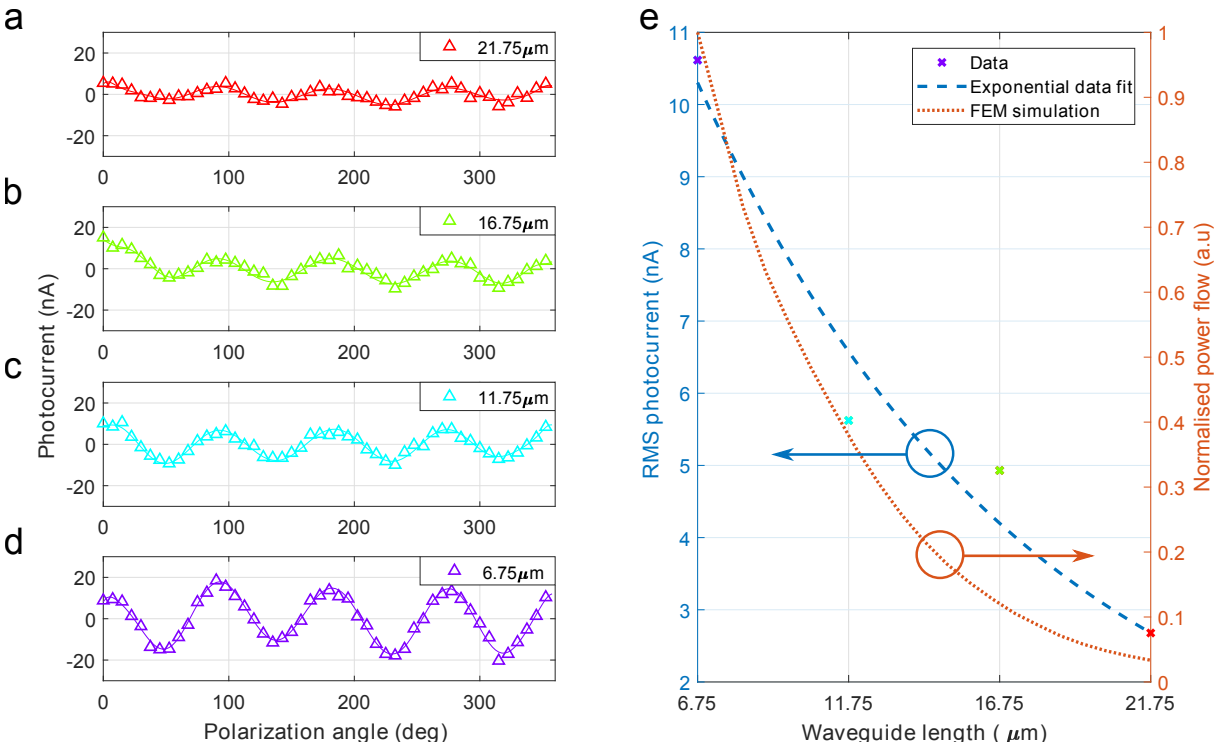

Figure 6: Photocurrent as a function of polarisation angle **(a-d)** for different waveguide lengths (mean value of the photocurrent is subtracted). Root mean square values of signals at each waveguide length (crosses) are shown on **(e)**. An exponential fit of the data (dashed line) and the normalised power flow at different distances along the 2.5 µm wide waveguide (dotted line) are plotted on the same graph, illustrating surface plasmon decay as it propagates along the waveguide.

the rotation of the half-wave plate. For normalisation purposes the dark current of each detector and the mean value of the photocurrent were subtracted from the output signals. Figures 6a-d show the relation between the registered photocurrent and the polarisation state of the incident beam for 21.75, 16.75, 11.75 and 6.75 µm long waveguides respectively. As can be seen, the amplitude of the signal decreases with increasing length which is in a good agreement with expectations. The lower responsivity of the photodetector coupled to the 11.75 µm long waveguide could be due to imperfections introduced during the fabrication stage.

The root mean square value of each signal as a function of the waveguide length is shown in Figure 6e together with the simulated normalised power flow along the 2.5 µm waveguide. Both curves show similar behaviour and reflect the decrease in RMS photocurrent as the waveguide length increases. Therefore, the measured exponential

dependence of the photocurrent with respect to waveguide length demonstrates that the device operates as a surface plasmon detector.

3 Conclusion and outlook

We proposed and experimentally demonstrated a novel planar surface plasmon detection technique which could form a component of future high-speed integrated optoelectronic circuits. The calculated theoretical bandwidth of the fabricated 13.75 μm^2 area MSM photodetector is of the order of 750 GHz. This value is well above the switching speed of the fastest silicon transistors, ensuring that the detection component will not be a limiting factor for the device. The performed optical (scattering, NSOM) and electrical (SPCM, photocurrent measurements) characterisations of a 2.5 μm wide waveguide-coupled MSM photodetector confirmed that the proposed device operates as a surface plasmon detector. The device fabrication is simple and can be compatible with a standard CMOS process. Additionally, since E-beam writing is suitable only for prototyping, a deep-UV lithography with phase-masks which is widely utilised in modern semiconductor fabrication will be more suitable for mass production. The structure presented in this work is flexible and permits varying the parameters such as the sizes of individual elements and materials to modify the operating wavelength. Although we used a grating coupler in our device, other surface plasmon excitation methods can be used to accommodate particular designs. Our technique can enable the integration of surface plasmons as signal carriers in future high-speed optoelectronic integrated circuits.

4 Acknowledgements

This research was supported under the Australian Research Council's Discovery Projects funding scheme (project number DP160100983). This work was performed in part at the Melbourne Centre for Nanofabrication (MCN) in the Victorian Node of the Australian National Fabrication Facility (ANFF). D.G. acknowledges the ARC for support through

a Future Fellowship (FT140100514).

4.0.1 Author contributions

E.P. conceived the concept, performed numerical simulations, fabricated and characterised the samples. J.J.C. assisted with fabrication. O.A. performed near-field scanning optical microscopy measurements. T.D.J., D.G., T.E. and A.R. provided oversight of the work. All authors discussed the experimental findings and analysis and contributed to writing the manuscript.

5 Methods

5.1 Simulations

Finite element method (FEM) analysis, implemented in COMSOL Multiphysics 5.2a with RF module, was used to simulate the excitation of surface plasmons as well as their propagation along the waveguide and decay in the MSM photodetector active area. Scattering boundary conditions terminate the model at all boundaries with an exception of an excitation port above the grating that was used to launch a polarised electromagnetic wave. A mesh with a maximum element size of 10 nm was used in the areas where a high simulation accuracy is desired (specifically the excitation grating, waveguide surface and MSM fingers). The optical properties of Au used in the model were taken from experimental data for bulk material [41].

5.2 Data availability

The data that support the plots within this paper and other findings of this study are available from the corresponding authors upon reasonable request.

5.3 Fabrication

Photodetectors and waveguides were fabricated on [100] n-type (phosphorus doped) silicon wafer with bulk resistivity of 1-10 Ω·cm. The wafer was covered with a 280 nm thick layer of PMMA A4 950k resist and exposed to create structures using a 100 kV EBPG5000+ electron beam lithography (EBL) system. The pattern was developed in 1:3 MIBK:IPA solution for 1 minute followed by 30 s rinsing in IPA and deionised water. The native oxide layer that might form during these steps was removed using 2% hydrofluoric (HF) acid and immediately loaded into an IntlVac NanoChrome II e-beam evaporator. The titanium adhesion layer with a thickness of 2 nm was deposited at 0.2 Å/s followed by 85 nm of gold deposited at 0.6 Å/s evaporation rates. After evaporation a lift-off step in hot acetone was performed. A wet dicing saw (Disco DAD321) was used to separate the photodetectors for packaging. The samples were glued into LCC20 ceramic packages and bonded using Kulicke & Soffa 4522D Ball bonder.

5.4 Characterisation

The device was characterized optically using a 635 nm Thorlabs S1FC635 Benchtop Fiber-Coupled Laser Source. A combination of polariser with half-wave plate was used to produce and control the linear polarisation of the beam. The half-wave plate AHWP05M-600 was mounted in a Thorlabs PRM1Z8 rotation stage. Utilisation of a Nikon CFI Plan Fluor x50 long working distance objective permitted the illumination of the coupling grating area. A polarisation insensitive 50:50 beam splitter (Thorlabs BS013) was used to align the beam. A Stanford Research Systems SR570 current preamplifier was used to bias and amplify the photocurrent generated by the detector. The amplification coefficient and biasing voltage were fixed during all measurements and set to be 10 nA/V and 0.15 V respectively. The signal from the amplifier was then sampled by a National Instruments USB-6343 DAQ.

A Thorlabs DCC1645C CMOS camera was used to collect bright-field and SPP scattering images of a photodetector.

Plasmonic waveguides were imaged using a Nanonics Multiview 2000 NSOM system. A 1064 nm laser was used to excite surface plasmons and an Au-covered NSOM probe (in collection mode) with an aperture diameter of 500 nm and resonance frequency of 32.4 kHZ was used to map the propagating plasmons.

For SPCM measurements the same laser was used together with a Nikon CFI Plan Fluor x100 long working distance objective to obtain a highly focused spot and to scan the device footprint. The resolution in both x and y directions was of approximately 100 nm.

References

[1] T.-B. Chiou, M. Dusa, A. C. Chen, D. Pietromonaco, *SPIE Advanced Lithography*, **2013**, pp. 86830R–86830R.

[2] W. Hafez, W. Snodgrass, M. Feng, *Applied Physics Letters* **2005**, *87*, 252109.

[3] E.-Y. Chang, C.-I. Kuo, H.-T. Hsu, C.-Y. Chiang, Y. Miyamoto, *Applied Physics Express* **2013**, *6*, 034001.

[4] A. Sinha, J. Cooper, H. Levinstein, *IEEE Electron Device Letters* **1982**, *3*, 90–92.

[5] D. Korn, *Silicon-Organic Hybrid Platform for Photonic Integrated Circuits*, *Vol. 15*, KIT Scientific Publishing, **2015**.

[6] M. T. Bohr, *International Electron Devices Meeting*, **1995**, pp. 241–244.

[7] R. Liu, C.-S. Pai, E. Martinez, *Solid-State Electronics* **1999**, *43*, 1003–1009.

[8] C. Diaz, K. Young, J. Hsu, J. Lin, C. Hou, C. Lin, J. Liaw, C. Wu, C. Su, C. Wang, *VLSI Technology, 1999. Digest of Technical Papers. 1999 Symposium on*, **1999**, pp. 11–12.

[9] P. Berini, *Physical Review B* **2000**, *61*, 10484.

[10] Y. Kurokawa, H. T. Miyazaki, *Physical Review B* **2007**, *75*, 035411.

[11] P. Neutens, P. Van Dorpe, I. De Vlaminck, L. Lagae, G. Borghs, *Nature Photonics* **2009**, *3*, 283–286.

[12] R. F. Oulton, V. J. Sorger, D. Genov, D. Pile, X. Zhang, *Nature Photonics* **2008**, *2*, 496–500.

[13] E. Panchenko, T. D. James, A. Roberts, *Journal of Nanophotonics* **2016**, *10*, 016019–016019.

[14] D. Ansell, I. Radko, Z. Han, F. Rodriguez, S. Bozhevolnyi, A. Grigorenko, *Nature communications* **2015**, *6*, year.

[15] W. Cai, J. S. White, M. L. Brongersma, *Nano Letters* **2009**, *9*, 4403–4411.

[16] J. A. Dionne, K. Diest, L. A. Sweatlock, H. A. Atwater, *Nano Letters* **2009**, *9*, 897–902.

[17] H. Lu, X. Liu, L. Wang, Y. Gong, D. Mao, *Optics Express* **2011**, *19*, 2910–2915.

[18] C. Marquart, S. Bozhevolnyi, K. Leosson, *Optics Express* **2005**, *13*, 3303–3309.

[19] S. A. Maier, *Plasmonics: Fundamentals and Applications*, Springer, **2007**.

[20] D. K. Gramotnev, S. I. Bozhevolnyi, *Nature Photonics* **2010**, *4*, 83–91.

[21] V. A. Zenin, A. Andryieuski, R. Malureanu, I. P. Radko, V. S. Volkov, D. K. Gramotnev, A. V. Lavrinenko, S. I. Bozhevolnyi, *Nano letters* **2015**, *15*, 8148–8154.

[22] W. L. Barnes, A. Dereux, T. W. Ebbesen, *Nature* **2003**, *424*, 824–830.

[23] J. J. Cadusch, T. D. James, A. Roberts, *Optics Express* **2013**, *21*, 28450–28455.

[24] J. J. Cadusch, T. D. James, A. Djalalian-Assl, T. J. Davis, A. Roberts, *Photonics Technology Letters IEEE* **2014**, *26*, 2357–2360.

[25] H. Wei, Z. Li, X. Tian, Z. Wang, F. Cong, N. Liu, S. Zhang, P. Nordlander, N. J. Halas, H. Xu, *Nano Letters* **2010**, *11*, 471–475.

[26] S. K. Earl, T. D. James, T. J. Davis, J. C. McCallum, R. E. Marvel, R. F. Haglund, A. Roberts, *Optics Express* **2013**, *21*, 27503–27508.

[27] S. K. Earl, T. D. James, R. E. Marvel, D. E. Gomez, T. J. Davis, J. G. Valentine, J. C. McCallum, R. F. Haglund, A. Roberts, *SPIE Micro+ Nano Materials, Devices, and Applications*, **2013**, pp. 89232S–89232S.

[28] B. Desiatov, I. Goykhman, N. Mazurski, J. Shappir, J. B. Khurgin, U. Levy, *Optica* **2015**, *2*, 335–338.

[29] Z. Han, I. P. Radko, N. Mazurski, B. Desiatov, J. Beermann, O. Albrektsen, U. Levy, S. I. Bozhevolnyi, *Nano letters* **2014**, *15*, 476–480.

[30] C. L. Smith, N. Stenger, A. Kristensen, N. A. Mortensen, S. I. Bozhevolnyi, *Nanoscale* **2015**, *7*, 9355–9386.

[31] M. Liu, E. Chen, S. Chou, *Applied Physics Letters* **1994**, *65*, 887–888.

[32] E. Panchenko, J. J. Cadusch, T. D. James, A. Roberts, *ACS Photonics* **2016**, *3*, 1833–1839.

[33] P. R. Berger, *Potentials IEEE* **1996**, *15*, 25–29.

[34] J. Lu, C. Petre, E. Yablonovitch, J. Conway, *JOSA B* **2007**, *24*, 2268–2272.

[35] H. Zimmermann, *Integrated Silicon Optoelectronics*, Springer, **2010**.

[36] A. Sobhani, M. W. Knight, Y. Wang, B. Zheng, N. S. King, L. V. Brown, Z. Fang, P. Nordlander, N. J. Halas, *Nature Communications* **2013**, *4*, 1643.

[37] D. L. Rogers, *Journal of Lightwave Technology* **1991**, *9*, 1635–1638.

[38] M. Aboelfotoh, K. Tu, *Physical Review B* **1986**, *34*, 2311.

[39] M. A. Taubenblatt, C. Helms, *Journal of Applied Physics* **1982**, *53*, 6308–6315.

[40] M. Barkelid, V. Zwiller, *Nature Photonics* **2014**, *8*, 47–51.

[41] P. B. Johnson, R.-W. Christy, *Physical Review B* **1972**, *6*, 4370.

Author/s:
Panchenko, E; Cadusch, JJ; Avayu, O; Ellenbogen, T; James, TD; Gomez, D; Roberts, A

Title:
In-Plane Detection of Guided Surface Plasmons for High-Speed Optoelectronic Integrated Circuits

Date:
2018-01-01

Citation:
Panchenko, E., Cadusch, J. J., Avayu, O., Ellenbogen, T., James, T. D., Gomez, D. & Roberts, A. (2018). In-Plane Detection of Guided Surface Plasmons for High-Speed Optoelectronic Integrated Circuits. ADVANCED MATERIALS TECHNOLOGIES, 3 (1), https://doi.org/10.1002/admt.201700196.